

REPORT DOCUMENTATION PAGE

Form Approved
OMB No. 0704-0188

Public reporting burden for this collection of information is estimated to average 1 hour per response, including the time for reviewing instructions, searching existing data sources, gathering and maintaining the data needed, and completing and reviewing this collection of information. Send comments regarding this burden estimate or any other aspect of this collection of information, including suggestions for reducing this burden to Department of Defense, Washington Headquarters Services, Directorate for Information Operations and Reports (0704-0188), 1215 Jefferson Davis Highway, Suite 1204, Arlington, VA 22202-4302. Respondents should be aware that notwithstanding any other provision of law, no person shall be subject to any penalty for failing to comply with a collection of information if it does not display a currently valid OMB control number. **PLEASE DO NOT RETURN YOUR FORM TO THE ABOVE ADDRESS.**

1. REPORT DATE (DD-MM-YYYY) 24-09-2007			2. REPORT TYPE Journal Article			3. DATES COVERED (From - To)		
4. TITLE AND SUBTITLE Numerical Study of Two-Phase Flow Field in a Simplified Swirl Cup Combustor (Preprint)						5a. CONTRACT NUMBER		
						5b. GRANT NUMBER		
						5c. PROGRAM ELEMENT NUMBER		
6. AUTHOR(S) Tae W. Park (AFRL/PRSA); Suresh K. Aggarwal (Univ. of Illinois); Viswanath R. Katta (Innovative Scientific Solutions); William M. Roquemore (AFRL/WPAFB)						5d. PROJECT NUMBER 23080532		
						5e. TASK NUMBER		
						5f. WORK UNIT NUMBER		
7. PERFORMING ORGANIZATION NAME(S) AND ADDRESS(ES) Air Force Research Laboratory (AFMC) AFRL/PRSA 10 E. Saturn Blvd. Edwards AFB CA 93524-7680						8. PERFORMING ORGANIZATION REPORT NUMBER AFRL-PR-ED-JA-2007-419		
9. SPONSORING / MONITORING AGENCY NAME(S) AND ADDRESS(ES) Air Force Research Laboratory (AFMC) AFRL/PRS 5 Pollux Drive Edwards AFB CA 93524-7048						10. SPONSOR/MONITOR'S ACRONYM(S)		
						11. SPONSOR/MONITOR'S NUMBER(S) AFRL-PR-ED-JA-2007-419		
12. DISTRIBUTION / AVAILABILITY STATEMENT Approved for public release; distribution unlimited (PA #07382A).								
13. SUPPLEMENTARY NOTES Submitted for publication in ASME Journal of Engineering for Gas Turbines and Power.								
14. ABSTRACT A numerical study was performed to investigate the two-phase flow field in a geometrically simplified swirl cup in a gas turbine combustor. The actual combustor has a hybrid-atomization feature with pressure atomization from the nozzle and airblast reatomization for the liquid film at the tip of venturi wall. The amount of liquid film formed in venturi tube could play an important role in characterizing the flow field of this combustor. Therefore, the major objective is to investigate the effects of swirl mode, gas temperature, and droplet injection characteristics on the amount of liquid film formed on the venturi wall. The present study first investigates the effects of the swirl mode and temperature of the primary and secondary air on the gas-phase flow field and then the effect of droplet injection characteristics in terms of velocity and location on the droplet transport and vaporization behavior. The detailed plots of droplet trajectory are used to identify the size ranges of the droplets which can form a liquid film by their impaction on the venturi tube wall. In general, the results indicate that the droplet injection characteristics have the dominant effect on the cut-off droplet diameter for droplet impaction on the venturi wall.								
15. SUBJECT TERMS								
16. SECURITY CLASSIFICATION OF:				17. LIMITATION OF ABSTRACT	18. NUMBER OF PAGES	19a. NAME OF RESPONSIBLE PERSON		
a. REPORT	b. ABSTRACT	c. THIS PAGE				19b. TELEPHONE NUMBER <i>(include area code)</i>		
Unclassified	Unclassified	Unclassified		SAR	29	N/A		

**NUMERICAL STUDY OF TWO-PHASE FLOW FIELD
IN A SIMPLIFIED SWIRL CUP COMBUSTOR (PREPRINT)**

TAE W. PARK*

Propulsion Directorate
Air Force Research Laboratory
Edwards AFB, CA 93524

SURESH K. AGGARWAL
University of Illinois at Chicago
Chicago, IL 60607

VISWANATH R. KATTA
Innovative Scientific Solutions, Inc
Dayton, OH 45430

and

WILLIAM M. ROQUEMORE
Propulsion Directorate
Air Force Research Laboratory
Wright-Patterson AFB, OH 45433

To Submit to **ASME Journal of Engineering for Gas Turbines and Power**

* Corresponding author

Phone: (661) 275-5165 Fax: (661) 275-6245

Email: tae.park@edwards.af.mil

Distribution A: Public release; distribution unlimited.

ABSTRACT

A numerical study was performed to investigate the two-phase flow field in a geometrically simplified swirl cup in a gas turbine combustor. The actual combustor has a hybrid-atomization feature with pressure atomization from the nozzle and airblast reatomization for the liquid film at the tip of venturi wall. The amount of liquid film formed in venturi tube could play an important role in characterizing the flow field of this combustor. Therefore, the major objective is to investigate the effects of swirl mode, gas temperature, and droplet injection characteristics on the amount of liquid film formed on the venturi wall. The present study first investigates the effects of the swirl mode and temperature of the primary and secondary air on the gas-phase flow field and then the effect of droplet injection characteristics in terms of velocity and location on the droplet transport and vaporization behavior. The detailed plots of droplet trajectory are used to identify the size ranges of the droplets which can form a liquid film by their impaction on the venturi tube wall. In general, the results indicate that the droplet injection characteristics have the dominant effect on the cut-off droplet diameter for droplet impaction on the venturi wall.

NOMENCLATURE

C_D	droplet drag coefficient
C_p	specific heat
g	gravitational acceleration
H	enthalpy
p	pressure
r	radial distance
Re_k	droplet Reynolds number
S_g^Φ	gas-phase source term for dependent variable Φ
t	time
T	temperature
u, v, w	axial, radial, and swirl velocity components
z	axial distance

Greek Symbols

Γ^Φ	transport coefficient in Eq. (1)
μ	dynamic viscosity
λ	thermal conductivity
ρ	density
Φ	dependent variable of Eq. (1)

Subscripts

g	gas-phase
k	droplet characteristic

INTRODUCTION

As is well known, liquid-fuel spray processes play a significant role in the performance of modern gas turbine combustors and industrial furnaces. Ignition, combustion stability, wall temperature, and pollutant emissions are strongly influenced by these processes (Lefebvre, 1983). As discussed by Gupta et al. (1984), introduction of swirl provides a recirculation zone which enhances mixing and flame stability.

Some high-performance aircraft engines such as in GE/SNECMA CFM56 engine combustor used a hybrid atomizer (Lefebvre, 1989) which is essentially a prefilming airblast atomizer with the addition of a simplex nozzle. It is designed to overcome a basic weakness of the pure airblast atomizer, namely poor atomization at the low air velocities associated with low cranking speeds. The simplex nozzle supplies pressure-atomized fuel to achieve rapid lightup during engine cranking and in the event of a flameout at high altitudes. Experiments (Wang et al., 1992; 1993; Jeng et al., 2004; Cai et al., 2007; Fu et al., 2007) and numerical analyses (Tolpadi, 1995; Tolpadi et al., 1995; Giridharan et al., 2003; Hsiao et al., 2003a; 2003b) have been conducted to characterize the gas-phase and liquid-phase flow fields downstream of a GE/SNECMA CFM56 engine combustor swirl cup in which the primary and secondary swirlers provide co-axial, counter-swirling airstreams. Due to the complexity of the co-axial, counter-

swirling air flows and the lack of adequate advanced diagnostics, a two-phase flow field with droplet vaporization in a hot gaseous environment has not been investigated in detail. Therefore, the overall objective of this paper is to study the transport and vaporization behavior of different-size droplets injected from the fuel nozzle in various two-phase flow fields.

Since the actual swirl cup simplified in our study involves hybrid atomization with a portion of liquid fuel impinging on venturi tube wall and getting reatomization, **a major consideration is to identify the parameter range for which the droplets impinge on the venturi tube wall.** An important parameter in this context is the minimum droplet diameter (d_{\min}), termed here as the cut-off diameter, for droplets to hit the venturi wall, i.e., droplets of diameter less than d_{\min} do not hit the venturi wall. The amount of liquid fuel formed in venturi tube could play an important role in characterizing the flow field of this combustor. Therefore, the trajectories of droplets become important consideration in assessing combustion performance.

The present study first investigates the effects of the swirl mode and temperature of the primary and secondary air on the gas-phase flow field and then the effect of droplet injection characteristics in terms of velocity and location on the droplet transport and vaporization behavior. The detailed plots of droplet trajectory are used to identify the size ranges of the droplets that can form a liquid film by their impaction on the venturi tube wall.

PHYSICAL AND NUMERICAL MODEL

We consider a simplified version of the GE swirl cup combustor that has been previously used in experimental study (Wang et al., 1992; 1993). As shown in Fig. 1, the simplified configuration consists of a spray nozzle, venturi tube, and flare tube. A simplex atomizer is mounted in the center of the swirl cup. It is important to note that although the numerical model considers a simplified combustor geometry

compared to the actual GE combustor, it employs a relatively wide range of parameters in order to simulate the realistic flow conditions. The numerical model is based on solving the time-dependent, two-phase equations in an axisymmetric geometry. The unsteady Navier-Stokes equations along with the conservation equations for enthalpy, turbulent-energy, and its dissipation rate in cylindrical (z, r) coordinate system are as follows:

$$\frac{\partial(\rho\Phi)}{\partial t} + \frac{\partial(\rho u\Phi)}{\partial z} + \frac{\partial(\rho v\Phi)}{\partial r} = \frac{\partial}{\partial z} \left(\Gamma^\Phi \frac{\partial\Phi}{\partial r} \right) + \frac{\partial}{\partial r} \left(\Gamma^\Phi \frac{\partial\Phi}{\partial z} \right) - \frac{\rho v\Phi}{r} + \frac{\Gamma^\Phi}{r} \frac{\partial\Phi}{\partial r} + S_s^\Phi + S_\ell^\Phi. \quad (1)$$

Here, ρ , u , v , and w are the density and the axial, radial, and swirl velocity components, respectively. Equation (1) represents different conservation equations, depending on the variable assigned to Φ . The source terms S^Φ and the transport coefficients Γ^Φ associated with each of these equations are given in Table 1.

In Table 1, μ , λ , and c_p are the viscosity, thermal conductivity, and specific heat, respectively, and μ_t is the turbulent viscosity incorporated through the k- ϵ turbulence model. The variables p , h , k , and ϵ are the pressure, enthalpy, and turbulent kinetic energy and its dissipation rate, respectively, and σ is the turbulent Prandtl number (or Schmidt number) associated with a specific transport equation. The other variables and constants appearing in the table are defined below:

$$G = \mu_t \left\{ 2 \left[\left(\frac{\partial u}{\partial z} \right)^2 + \left(\frac{\partial v}{\partial r} \right)^2 + \left(\frac{v}{r} \right)^2 \right] + \left(\frac{\partial v}{\partial z} + \frac{\partial u}{\partial r} \right)^2 + \left(\frac{\partial w}{\partial z} \right)^2 + \left(\frac{\partial w}{\partial r} - \frac{w}{r} \right)^2 \right\}$$

$$\mu_t = C_\mu \rho k^2 / \epsilon$$

$$C_1 = 1.44, C_2 = 1.92, \text{ and } C_\mu = 0.09$$

$$\sigma_k = 1.0, \sigma_\epsilon = 1.21, \text{ and } \sigma_h = 0.9$$

Temperature-dependent thermodynamic and transport properties are used in this formulation. The enthalpy is calculated from polynomial curve-fits, while the viscosity, thermal conductivity, and diffusion coefficients are estimated from the Leonard-Jones potentials.

Flat velocity profiles are used at the air inflow boundaries. A simple extrapolation procedure (Katta et al., 1994b) with weighted zero- and first-order terms was used to estimate the flow variables at the outflow boundary. The usual no-slip, adiabatic boundary conditions were applied at the walls. Wall functions were used for determining the gradients of the flow variables near the walls.

Density is obtained by solving the state equation, while the pressure field at every time step is determined from pressure Poisson equations. For the cases in which turbulent-flow characteristics were modeled, the time-dependent equations for turbulent energy (k) and turbulent-energy dissipation rate (ϵ) are also solved, along with the other governing equations. The standard isotropic k - ϵ turbulence model is incorporated in those cases. Even though all the governing equations are solved in an uncoupled manner, the turbulence-conservation equations are coupled through the source terms during the solution process to improve the stability of the algorithm.

An orthogonal, staggered-grid system with varying cell sizes in both the z and r directions is utilized. The momentum equations are integrated using an implicit QUICKEST (Quadratic Upstream Interpolation for Convective Kinematics with Estimated Streaming Terms) numerical scheme (Katta et al., 1994a; Leonard, 1979) which is third-order accurate in both space and time and has a very low numerical diffusion error. On the other hand, the enthalpy and turbulence-energy conservation equations, which have relatively large source terms, are integrated using the hybrid scheme of Spalding (1972). By rearrangement of the terms, the finite-difference form of each governing equation at all grid points is written as a system of algebraic equations which is then solved using the Alternative-Direction-Implicit

(ADI) technique. The time increment, Δt , is determined from the stability constraint and maintained as a constant during the entire calculation. The pressure field at every time step is accurately calculated by simultaneously solving the system of algebraic pressure Poisson equations at all grid points using the LU (Lower-Upper) decomposition technique.

The Lagrangian approach is employed to solve the liquid-phase governing equations for the dynamics of each droplet group. The spray is characterized by a discrete number of droplet groups, distinguished by their injection location, initial size, and time of injection. The equations governing the variation of position and velocity of each droplet are as follows:

$$\begin{aligned}\frac{dx_k}{dt} &= u_k \\ \frac{dy_k}{dt} &= v_k\end{aligned}\tag{2}$$

$$\begin{aligned}\frac{du_k}{dt} &= \frac{3C_D\rho_g}{4d_k\rho_k}|u_g - u_k|(u_g - u_k) + \left(\frac{\rho_g}{\rho_k} - 1\right)g \\ \frac{dv_k}{dt} &= \frac{3C_D\rho_g}{4d_k\rho_k}|v_g - v_k|(v_g - v_k) + \frac{w_k^2}{y_k} \\ \frac{dw_k}{dt} &= \frac{3C_D\rho_g}{4d_k\rho_k}|w_g - w_k|(w_g - w_k) - \frac{v_k w_k}{y_k}\end{aligned}\tag{3}$$

where

$$C_D = \frac{24}{\text{Re}_k} \left(1 + \frac{\text{Re}_k^{2/3}}{6} \right)\tag{4}$$

$$\text{Re}_k = \frac{\rho_g \left\{ (u_g - u_k)^2 + (v_g - v_k)^2 + (w_g - w_k)^2 \right\}^{1/2} d_k}{\mu_g} \quad (5)$$

Other expressions concerning droplet evaporation can be found in our previous paper (Park et al., 1995).

Axisymmetric calculations are made on a physical domain of 76 mm in radial direction and 126 mm in axial direction. A nonuniform grid system with 211×121 grid points, with a large number of grid points clustered in the shear layer (boundary of different flow regions) and at the bodies and walls, are utilized to resolve the steep gradients of the dependent variables. The computational domain is bounded by the axis of symmetry and an outflow boundary in the radial direction and by the inflow and another outflow boundary in the axial direction. The outer boundaries in the z and r directions are located sufficiently far from the nozzle and swirler exit and the axis of symmetry, respectively, to minimize the propagation of boundary-induced disturbances into the region of interest. For the given flow conditions, a solution of steady-state gas-phase flowfield is obtained for the calculation of 20,000 time steps. Then, a solution of liquid-phase flowfield is obtained for the calculation of 2,000 time steps using the steady-state gas-phase flowfield.

The liquid-phase equations governing the position and velocity of each droplet group are advanced in time by a second-order accurate Runge-Kutta method. Since the gas-phase solution employs an implicit procedure, the temporal step size used for integrating the liquid-phase equations is usually smaller than that for gas-phase equations. An automatic procedure is implemented in order to select an optimum liquid-phase time step. The procedure to advance the two-phase solution over one gas-phase time step is as follows. Using the known gas-phase properties, the liquid-phase equations are solved over the specified number of liquid-phase subcycles. A third-order accurate Lagrangian polynomial method is used for interpolating the gas-phase properties from the nonuniform fixed grid to the droplet characteristic location. It should be noted that the interpolation scheme for the gas-phase velocities u and

v is based on their respective grid cells because of the use of a staggered grid in gas-phase calculation. The droplet properties are updated after every liquid-phase subcycle.

RESULTS AND DISCUSSION

Gas-Phase Results. The gas-phase flow field was simulated for six different flow conditions in terms of temperature and swirl. Six different cases listed in Table 2 are selected to investigate the effects of swirl and temperature on flow structure, especially with regard to the number and size of the recirculation zones, and droplet transport in the swirl cup combustor. Since swirl plays a central role in characterizing the flow and stabilizing the flame, it is very important to investigate the effect of different modes of swirl on the structure of both cold and hot flow in the combustor. Three different modes of swirl are chosen for this purpose as shown in Table. 2. As indicated in the table, the first three cases represent a cold flow with three different modes of swirl, namely nonswirling, co-swirling and counter-swirling primary and secondary air streams. The next three cases present a hot flow for the same three modes of swirl. The conditions for temperature and swirl velocity for these six cases are listed in the table. The effective Reynolds numbers based on the velocity and the width of primary air flow are 10,128 and 928 for cold and hot flow, respectively. Note that the density is reduced by a factor of 4.2 times and the viscosity is increased by a factor of 2.6 times for the hot cases.

Figure 2 shows the steady-state solutions for three different turbulent cold flows in the form of velocity vectors in the left half and streamlines in the right half. One large central recirculation zone is created downstream of the combustor and extended up to $z = 19.7$ mm for the nonswirling case as shown in Fig. 2(a). The size and shape of this central (primary) recirculation zone (created by the primary air flow) are drastically modified for the swirling cases due to the adverse pressure gradient effect of swirl. The axial size of the central recirculation zone is reduced from 19.7 mm to 5 mm for both the swirl cases. The radial size is also significantly reduced for the swirling cases. In addition, for both the swirling cases,

the primary recirculation zone generates a secondary recirculation zone between the primary zone and central line. Thus, it appears that the flow field immediately downstream of the nozzle wall ($r_{\text{wall}} = 2\text{-}4.68$ mm) is strongly modified due to swirl in the primary stream. Another major effect of swirl is the appearance of a third recirculation zone in the downstream region. However, the size and shape of this recirculation zone are noticeably different for the co-swirling and counter-swirling cases. The axial size is 6 mm for the co-swirling case, whereas it is 11 mm for counter-swirling case. In the radial direction, the recirculation zone extends from 3 mm to the central line for the former case, whereas it extends from 3 mm to 1.5 mm for the latter.

Simulating hot flows in the combustor is more realistic and closer to the real operating conditions. Consequently, we consider a high-temperature case to examine the effects of temperature on flow structure for the three modes of swirl discussed above. Figure 3 shows the velocity vector plots and streamlines for hot nonswirling, co-swirling and counter-swirling flows. For the nonswirling case, the length of the central recirculation zone is considerably reduced due to the effect of temperature, caused primarily by the reduction in the effective Reynolds number. In addition, the vortex shedding that is observed in the downstream region of the first body is significantly weakened due to the effect of temperature. The comparison of results for the hot and cold swirling cases indicates that the third recirculation zone completely disappears for the co-swirling hot case, while its size is reduced for the counter-swirling hot case compared to the corresponding cold swirling cases.

The heights of central recirculation zones for the previous cold cases are clearly shown in Fig. 4(a) by plotting axial velocities at the centerline. Those are 19.7, 5, 15 mm for nonswirling, co-swirling, and counter-swirling cases, respectively. Also, maximum negative axial velocities for the corresponding cases are -13.4, -0.9, -4.7 m/s, respectively. The radial profiles of axial velocity at axial location of 3 mm also captured the secondary recirculation zones only for the swirling cases.

Figure 5(a) shows the heights of the central recirculation zones for the hot flows, which are 16.6 and 7.8 mm for nonswirling and counter-swirling cases, respectively. The maximum negative velocities for the corresponding two cases are -13.8 and -1.3 m/s, respectively. The effect of central recirculation zone on the temperature flow field near nozzle exit is clearly shown in Fig. 5(b) by radial temperature profiles at axial location of 3 cm.

Liquid-Phase Results. These results focus on the transport of nonevaporating and evaporating droplets in the swirling flow fields discussed earlier. Since the GE swirl cup involves hybrid atomization with a portion of liquid fuel impinging on venturi tube wall and getting reatomization, a major consideration is to identify the parameter range for which the droplets impinge on the venturi wall. An important parameter in this context is the minimum droplet diameter (d_{\min}), termed here as the cut-off diameter, for droplets to hit the venturi wall, i.e., droplets of diameter less than d_{\min} do not hit the venturi wall. The cut-off diameter is expected to be dependent on the gas- and liquid-phase parameters. The gas-phase parameters include such as swirl number, co-swirl or counter-swirl, gas temperature and turbulence characteristics. The liquid-phase parameters would include spray injection characteristics such as spray cone angle, and droplet size and velocity distributions. In the following, we report results of a limited parametric study to examine the dependence of d_{\min} on different parameters such as injection velocity, swirl, gas temperature, and vaporization. To simulate the spray injection process, we consider 9 different droplet sizes (10, 20, 30, 40, 50, 75, 100, 150, 200 μm) and 4 different droplet injection velocities (1, 5, 10, 20 m/s) with a fixed spray cone angle of 90 degree. One injection location ($r_{\text{inj}} = 2$ mm) is considered for the cold flow cases. However, for the hot flow cases, two different injection locations ($r_{\text{inj}} = 0.2, 2$ mm) are chosen to obtain more significant changes in evaporating droplet trajectories due to increased droplet residence time.

Figure 6 shows the trajectories of different-size, nonevaporating droplets for two different injection velocities and three different swirl modes. Since the gas flow field is steady, the trajectories can be represented by plotting instantaneous locations of different-size droplets, shown for injection velocities of 5 and 20 m/s on the left and right side of the central line, respectively. The trajectories are computed from $t = 0.0383\text{-}0.0421$ s by solving the gas-phase and the droplet equations simultaneously. Seven droplet sizes of 10, 20, 30, 40, 50, 75, 150 μm are represented in these figures. As mentioned earlier, droplets are injected at spray nozzle rim with 45 degree injection angle. For the nonswirling case shown in Fig. 6(a), the cut-off diameter (d_{\min}) is between 60-65 μm for injection velocity of 5 m/s, and 20-25 μm for injection velocity of 20 m/s. The trajectory of 10- μm droplet with lower injection velocity is strongly affected by gas flow especially near region of nozzle exit. The trajectories of non-evaporating droplets in co-swirling and counter-swirling turbulent flows are shown in Fig. 6(b) and 6(c), respectively. Although there is no change in cut-off diameters for the corresponding cases, the droplet trajectories are significantly modified by swirl. The trajectories of all droplets are strongly modified by swirl, especially in recirculation zones near the nozzle exit. Droplets are dispersed radially outward due to swirl. This implies that the droplet distribution is significantly altered by swirl. For the lower injection velocity, the cut-off diameter is larger for the swirling cases compared to that for the nonswirling case while for the high injection velocity, that does not seem to be affected due to the reduced droplet residence time.

The trajectories of evaporating droplets for the different gas-phase swirl mode and droplet injection velocities are portrayed in Fig. 7. In our simulation, evaporation is terminated when the droplet size becomes 5 μm regardless of its initial size. Again, in each figure, the droplet trajectories for the injection velocity of 5 m/s and 20 m/s are plotted on the left half and right half, respectively. The cut-off diameters for the low injection velocity (5 m/s) for the nonswirling, co-swirling, and counter-swirling flows are 45-50, 50-55, and 50-55 μm , respectively while those for the high injection velocity (20 m/s)

for the corresponding flows are 15-20, 20-25, 20-25 μm , respectively. The droplets are more vaporized for the low injection velocity case due to increased droplet residence time. Increasing injection velocity results in a reduction of the cut-off droplet diameter. This implies more droplets would impinge on the venturi tube wall and liquid film thickness on the wall would be increased. It is important to characterize the liquid film formed by droplets impinging on the wall. It means that more liquid films are formed on the first body for the case of smaller cut-off droplet size. It is very important to characterize the amount of liquid film formed by droplets impinging onto the wall, since the swirl strength of the primary and secondary streams can be optimized for the desired reatomization of the liquid film at the venturi tube tip in this particular hybrid-type atomizer combustor.

Figure 8 shows the trajectories of evaporating droplets for two different swirl modes when they are injected at radial location of 0.2 mm. The cut-off diameters for the low injection velocity for nonswirling and counter-swirling flows are 55-60 μm and 65-70 μm , respectively while those for the high injection velocity for the corresponding flows are 20-25 μm regardless of the swirl mode. For the droplet injection close to the center, the droplet residence time is increased, which increased significantly the cut-off droplet diameter for low injection velocity (5 m/s).

In summary, Table 3 shows cut-off droplet sizes for all cases presented in the previous section. More droplets diameters (55, 60, 65, 70 μm for 5 m/s injection velocity and 25 μm for 20 m/s injection velocity) were considered in the simulations for all the cases to obtain more specific cut-off droplet diameters.

CONCLUSIONS

A numerical study has been performed to investigate the two-phase flow field in a geometrically simplified swirl cup in a gas turbine combustor. The actual combustor has a hybrid-atomization feature

with pressure atomization from the nozzle and airblast reatomization for the liquid film at the tip of venturi wall. The amount of fuel formed in venturi tube could play an important role in characterizing the flow field of this combustor. The present study first investigates the effects of the swirl mode and temperature of the primary and secondary air on the gas-phase flow field and then the effect of droplet injection characteristics in terms of velocity and location on the droplet transport and vaporization behavior. The results indicate that the gas-phase flow field is strongly modified due to swirl in the primary stream. Another major effect of swirl on the gas-phase structure is the appearance of a third recirculation zone in the downstream region. The size and shape of this recirculation zone are noticeably different for the co-swirling and counter-swirling cases. The detailed plots of droplet trajectory are used to successfully identify the size ranges of the droplets which can form a liquid film by their impaction on the venturi tube wall. Increasing injection velocity results in a reduction of the cut-off droplet diameter for all cases with a different swirl mode and temperature. For the low injection velocity (5 m/s), the cut-off diameter is greater for the swirling cases compared to that of nonswirling case while for the high injection velocity (10, 20 m/s), that does not seem to be changed due to the decreased droplet residence time. For the droplet injection location close to the center, the droplet residence time is increased, which significantly increases the cut-off droplet diameter for 5 m/s injection velocity. In general, the results indicate that the droplet injection characteristics have the dominant effect on the cut-off droplet diameter for droplet impaction on the venturi wall.

ACKNOWLEDGMENTS

This work was supported by the National Research Council and the Air Force Research Laboratory.

REFERENCES

Cai, J., Fu, Y., Flohre, N., Jeng, S.-M., and Mongia, H., 2007, "Experimental Study on Coherent Structures of a Counter-rotating Multi-Swirl Cup," AIAA Paper 2007-5674, 43rd AIAA/ASME/SAE/ASEE Joint Propulsion Conference & Exhibit, Cincinnati, OH.

- Fu, Y., Cai, J., Jeng, S.-M., and Mongia, H., 2007, "Characteristics of the Swirling Flow Generated by a Counter-rotating Swirler," AIAA Paper 2007-5690, 43rd AIAA/ASME/SAE/ASEE Joint Propulsion Conference & Exhibit, Cincinnati, OH.
- Giridharan, M. G., Mongia, H., and Jeng, S.-M., 2003, "Swirl Cup Modeling – Part VIII: Spray Combustion in CFM-56 Single Cup Flame Tube," AIAA Paper 2003-319, 41st AIAA Aerospace Sciences Meeting & Exhibit, Reno, NV.
- Gupta, A. K., Lilley, D. G., and Syred, N., 1984, "Swirl Flows," Abacus Press, pp. 1-2.
- Hsiao, G., Mongia, H., and Vij, A., 2003a, "Swirl Cup Modeling – Part II: Inlet Boundary Conditions," AIAA Paper 2003-1350, 41st AIAA Aerospace Sciences Meeting & Exhibit, Reno, NV.
- Hsiao, G. and Mongia, H., 2003b, "Swirl Cup Modeling – Part III: Grid Independent Solution with Different Turbulence Models," AIAA Paper 2003-1349, 41st AIAA Aerospace Sciences Meeting & Exhibit, Reno, NV.
- Jeng, S.-M., Flohre, N. M., and Mongia, H., 2004, "Swirl Cup Modeling - Atomization," AIAA Paper 2004-137, 42nd AIAA Aerospace Sciences Meeting & Exhibit, Reno, NV.
- Katta, V. R., Goss, L. P., and Roquemore, W. M., 1994a, "Numerical Investigations of Transitional H₂/N₂ Jet Diffusion Flames," AIAA Journal, Vol. 32, pp. 84-94.
- Katta, V. R., Goss, L. P., and Roquemore, W. M., 1994b, "Simulation of Vortical Structures in a Jet Diffusion Flame," Int. J. Num. Meth. Heat Fluid Flow, Vol. 4, pp. 413.
- Lefebvre, A. H., 1983, "Gas Turbine Combustion," Hemisphere Publishing Corp., Washington, D.C., pp. 371-391.
- Lefebvre, A. H., 1989, "Atomization and Sprays," Hemisphere Publishing Corp., Washington, D.C., pp. 140-142.
- Leonard, B. P., 1979, "A Stable and Accurate Convective Modelling Procedure Based on Quadratic Upstream Interpolation," Computational Methods in Applied Mechanics and Engineering, Vol. 19, pp. 59-98.
- Park, T. W., Aggarwal, S. K., and Katta, V. R., 1995, "Gravity Effects on the Dynamics of Evaporating Droplets in a Heated Jet," Journal of Propulsion and Power, Vol. 11, pp. 519-528.
- Spalding, D. B., 1972, "A Novel Finite Difference Formulation for Difference Expressions involving both First and Second Derivatives," Int. J. for Numerical Methods in Engineering, Vol. 4, pp. 551-559.
- Tolpadi, A. K., 1995, "Calculation of Two-phase Flow in Gas Turbine Combustors," Journal of Engineering for Gas Turbines and Power, Vol. 117, pp. 695-703.
- Tolpadi, A. K., Burrus, D. L., and Lawson, R. J., 1995, "Numerical Computation and Validation of Two-Phase Flow Downstream of a Gas Turbine Combustor Dome Swirl Cup," Journal of Engineering for Gas Turbines and Power, Vol. 117, pp. 704-712.

Wang, H. Y., McDonell, V. G., and Samuelsen, G. S., 1992, "The Two-Phase Flow Downstream of a Production Engine Combustor Swirl Cup," Twenty-Fourth Symposium (International) on Combustion, The Combustion Institute, Pittsburgh, PA, pp. 1457-1463.

Wang, H. Y., McDonell, V. G., Sowa, W. A., and Samuelsen, G. S., 1993, "Scaling of the Two-Phase Flow Downstream of a Gas Turbine Combustor Swirl Cup: Part I-Mean Quantities," Journal of Engineering for Gas Turbines and Power, Vol. 115, pp.453-460.

Table 1: Transport coefficients and source terms appearing in governing equations

Φ	Γ^Φ	S^Φ
1	0	0
u	$\mu + \mu_t$	$-\frac{\partial p}{\partial z} + \frac{\partial}{\partial z} \left(\Gamma^u \frac{\partial u}{\partial z} \right) + \frac{\partial}{\partial r} \left(\Gamma^u \frac{\partial v}{\partial z} \right) + \frac{\Gamma^u}{r} \frac{\partial v}{\partial z} - \frac{2}{3} \left[\frac{\partial}{\partial z} \left(\Gamma^u \frac{\partial u}{\partial z} \right) + \frac{\partial}{\partial z} \left(\Gamma^u \frac{\partial v}{\partial r} \right) + \frac{\partial}{\partial z} \left(\Gamma^u \frac{v}{r} \right) \right]$
v	$\mu + \mu_t$	$-\frac{\partial p}{\partial r} + \frac{\partial}{\partial z} \left(\Gamma^v \frac{\partial u}{\partial r} \right) + \frac{\partial}{\partial r} \left(\Gamma^v \frac{\partial v}{\partial r} \right) + \frac{\Gamma^v}{r} \frac{\partial v}{\partial r} - 2\Gamma^v \frac{v}{r^2} + \rho \frac{w^2}{r} - \frac{2}{3} \left[\frac{\partial}{\partial r} \left(\Gamma^v \frac{\partial u}{\partial z} \right) + \frac{\partial}{\partial r} \left(\Gamma^v \frac{\partial v}{\partial r} \right) + \frac{\partial}{\partial r} \left(\Gamma^v \frac{v}{r} \right) \right]$
w	$\mu + \mu_t$	$-\left(\frac{\Gamma^w}{r^2} + \rho \frac{v}{r} + \frac{1}{r} \frac{\partial \Gamma^w}{\partial r} \right) w$
k	$\mu + \frac{\mu_t}{\sigma_k}$	$G - \rho \varepsilon$
ε	$\mu + \frac{\mu_t}{\sigma_\varepsilon}$	$C_1 G \frac{\varepsilon}{k} - C_2 \rho \frac{\varepsilon^2}{k}$
H	$\frac{\lambda}{C_p} + \frac{\mu_t}{\sigma_H}$	0

Table 2: Flow conditions of the present simulations

Case	Air Flows	Inlet Velocity (m/s)			Inlet Temp. (K)
		u	v	w	T
I	Primary	38	0	0	289
	Secondary	35	0	0	289
II	Primary	38	0	19	289
	Secondary	35	0	17.5	289
III	Primary	38	0	19	289
	Secondary	35	0	-17.5	289
IV	Primary	38	0	0	1200
	Secondary	35	0	0	1200
V	Primary	38	0	19	1200
	Secondary	35	0	17.5	1200
VI	Primary	38	0	19	1200
	Secondary	35	0	-17.5	1200

Table 3: Cut-off droplet diameters for various cases

Injection Velocity	Cold, No-Swirl	Cold, Co-Swirl	Cold, Counter-Swirl	Hot, No-Swirl	Hot, Co-Swirl	Hot, Counter-Swirl	Hot ¹ , No-Swirl	Hot ¹ , Counter-Swirl
1 m/s	infinity	infinity	infinity	infinity	*	infinity	infinity	infinity
5	60-65 μm	70-75	65-70	45-50	50-55	50-55	55-60	65-70
10	30-35	30-35	30-35	30-35	30-35	30-35	30-35	30-35
20	20-25	20-25	20-25	15-20	20-25	20-25	20-25	20-25

Superscript 1 represents the cases with the injection location close to the center.

* indicates that no clear d_{\min} is found and only 50- μm droplet impinges on the wall which requires further explanation.

List of Figures

- Figure 1: Schematics of the simplified combustor swirl cup.
- Figure 2: Velocity vectors and streamlines for a cold turbulent flow with three different swirl modes: (a) no-swirl, (b) co-swirl, and (c) counter-swirl.
- Figure 3: Velocity vectors and streamlines for a hot turbulent flow with three different swirl modes: (a) no-swirl, (b) co-swirl, and (c) counter-swirl.
- Figure 4: (a) Axial profiles of gas-phase axial velocity along symmetry axis, and (b) radial profiles of gas-phase axial velocity at $z = 3$ mm for the three swirl cases for the primary and secondary cold air flows.
- Figure 5: (a) Axial profiles of gas-phase axial velocity along symmetry axis, and (b) radial profiles of gas-phase temperature and axial velocity at $z = 3$ mm for the three swirl cases for the primary and secondary heated air flows.
- Figure 6: Trajectories of non-evaporating droplets injected at $r_{inj} = 2$ mm for a cold turbulent flow with three different swirl modes: (a) no-swirl, (b) co-swirl, and (c) counter-swirl. In each figure, trajectories are shown for injection velocities of 5 and 20 m/s on the left and right side of the central line, respectively.
- Figure 7: Trajectories of evaporating droplets injected at $r_{inj} = 2$ mm for a hot turbulent flow with three different swirl modes: (a) no-swirl, (b) co-swirl, and (c) counter-swirl. In each figure, trajectories are shown for injection velocities of 5 and 20 m/s on the left and right side of the central line, respectively.
- Figure 8: Trajectories of evaporating droplets injected at $r_{inj} = 0.2$ mm for a hot turbulent flow with two different swirl modes: (a) no-swirl, (b) counter-swirl. In each figure, trajectories are shown for injection velocities of 5 and 20 m/s on the left and right side of the central line, respectively.

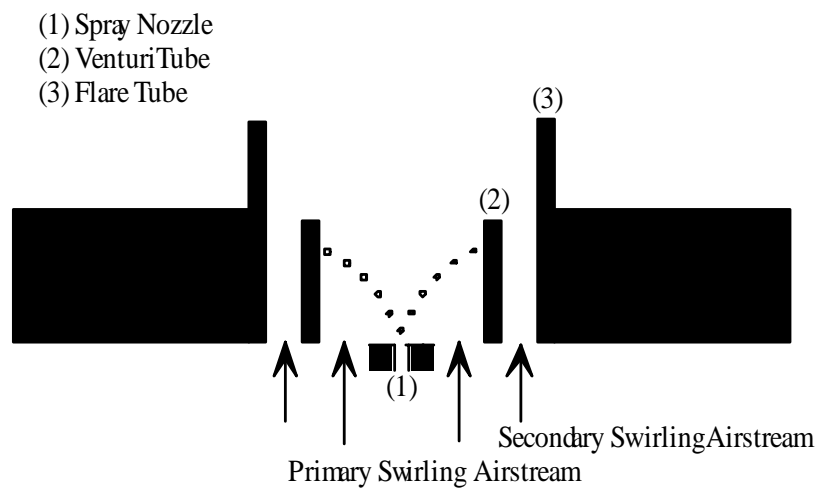


Fig. 1 Schematics of the simplified combustor swirl cup.

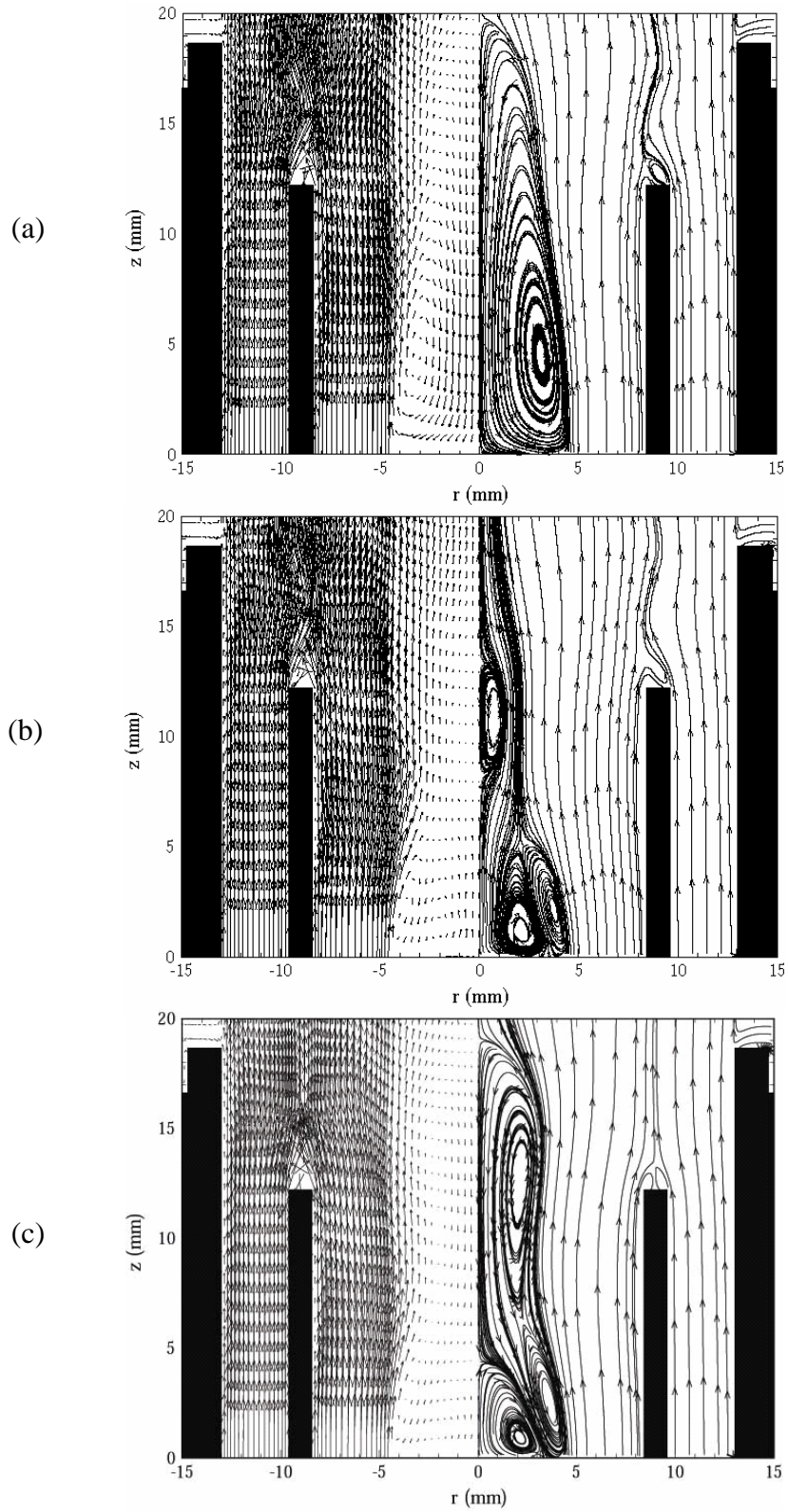


Fig. 2 Velocity vectors and streamlines for a cold turbulent flow with three different swirl modes: (a) no-swirl, (b) co-swirl, and (c) counter-swirl.

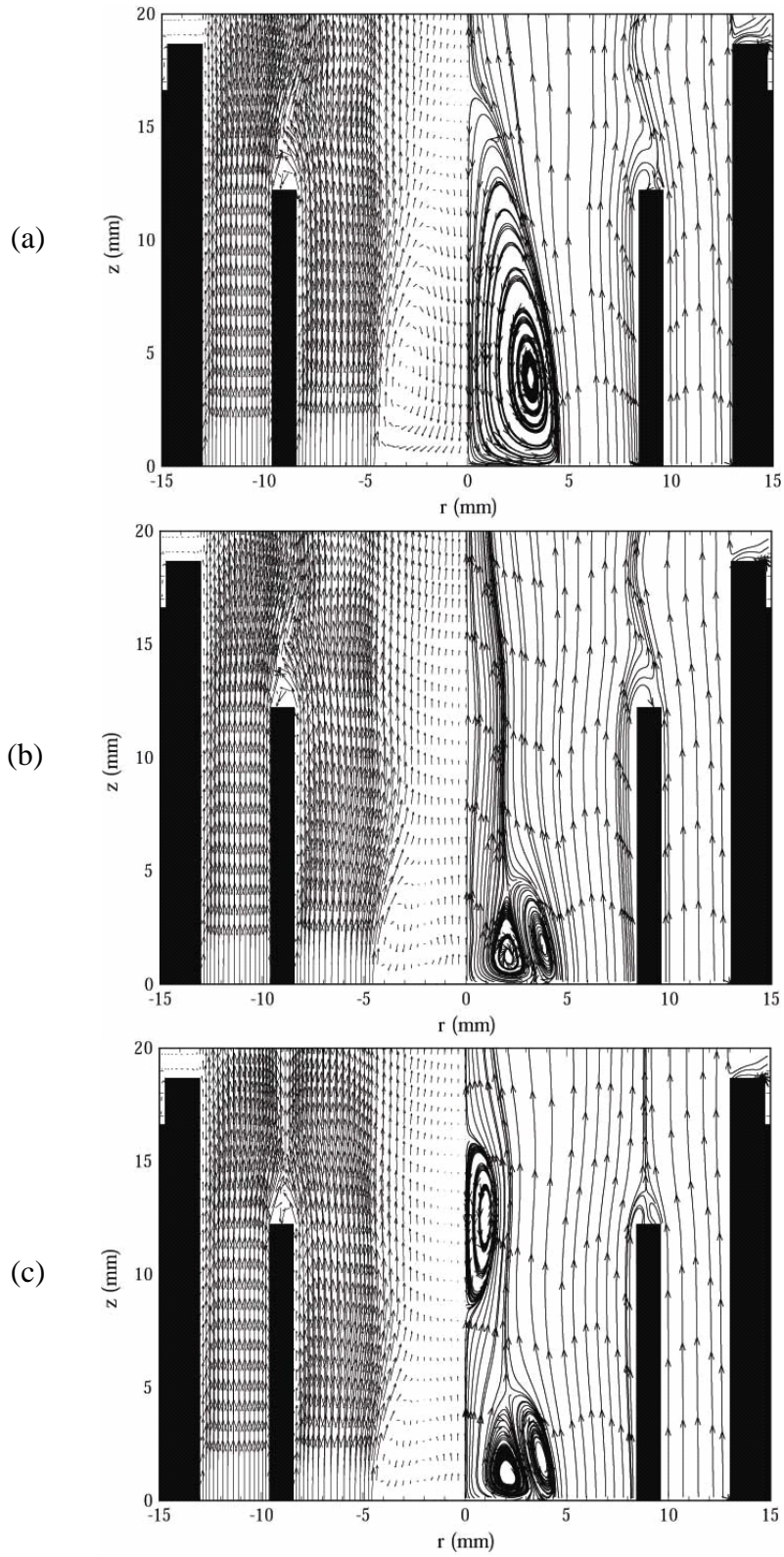


Fig. 3 Velocity vectors and streamlines for a hot turbulent flow with three different swirl modes: (a) no-swirl, (b) co-swirl, and (c) counter-swirl.

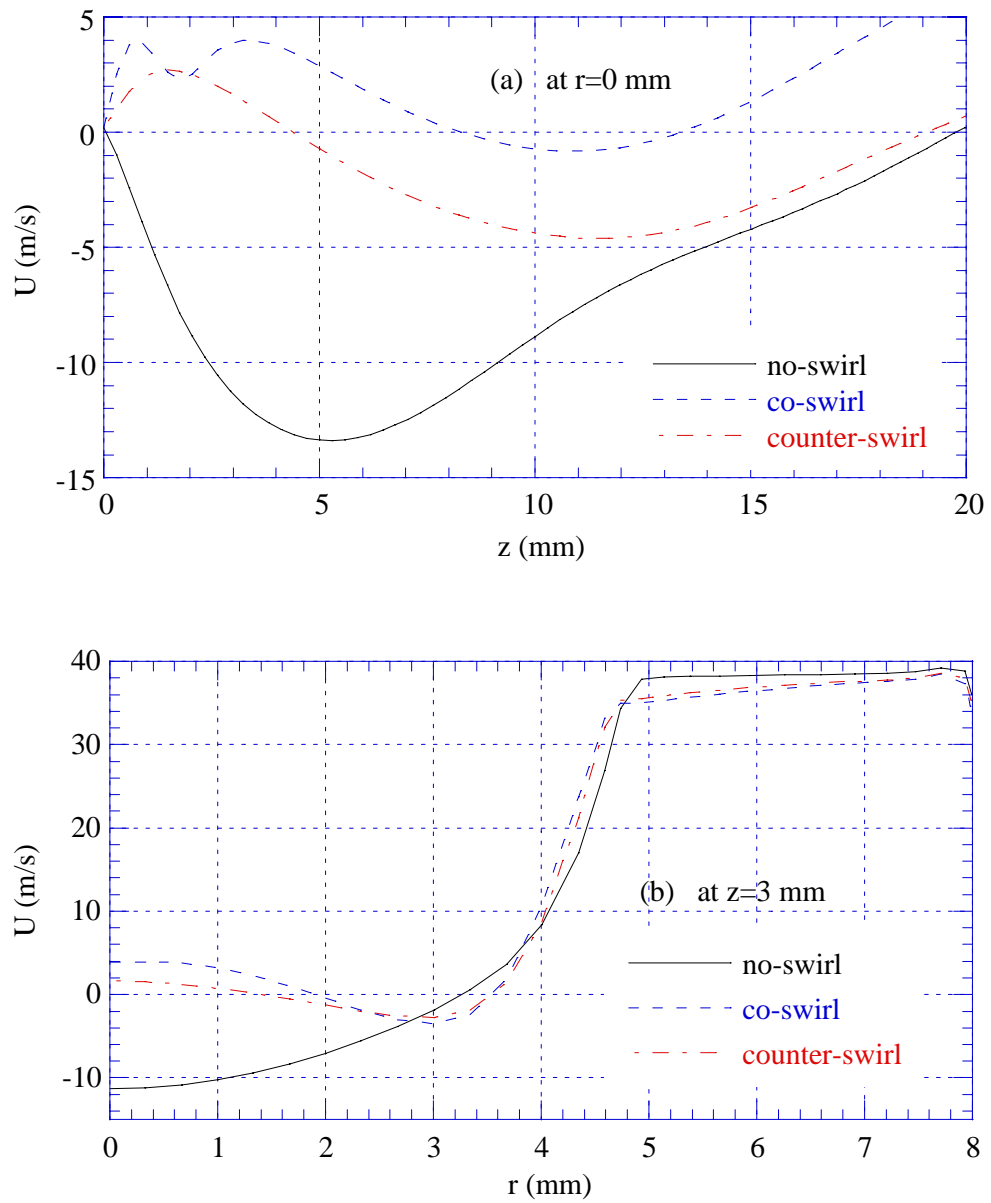


Fig. 4 (a) Axial profiles of gas-phase axial velocity along symmetry axis, and (b) radial profiles of gas-phase axial velocity at $z = 3$ mm for the three swirl cases for the primary and secondary cold air flows.

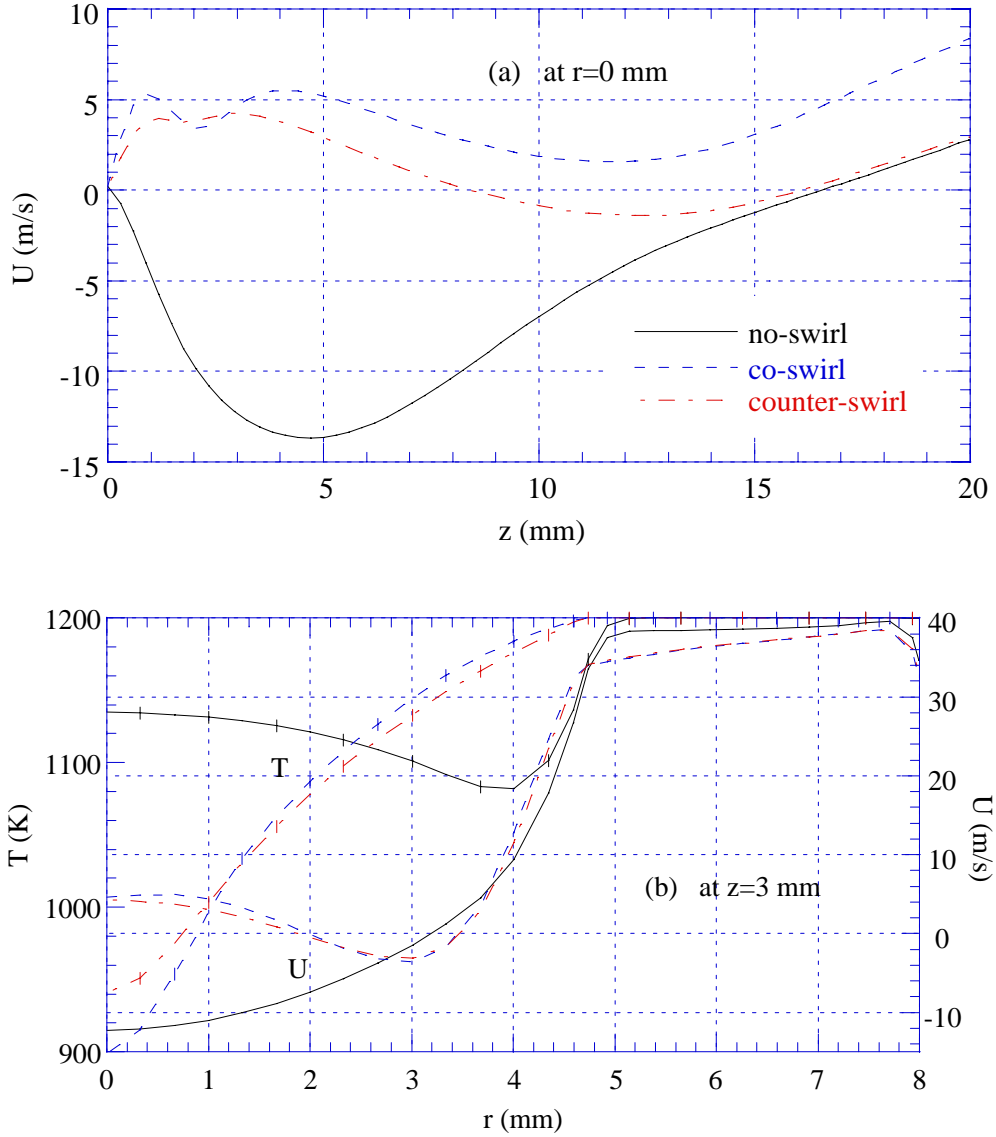


Fig. 5 (a) Axial profiles of gas-phase axial velocity along symmetry axis, and (b) radial profiles of gas-phase temperature and axial velocity at $z = 3$ mm for the three swirl cases for the primary and secondary heated air flows.

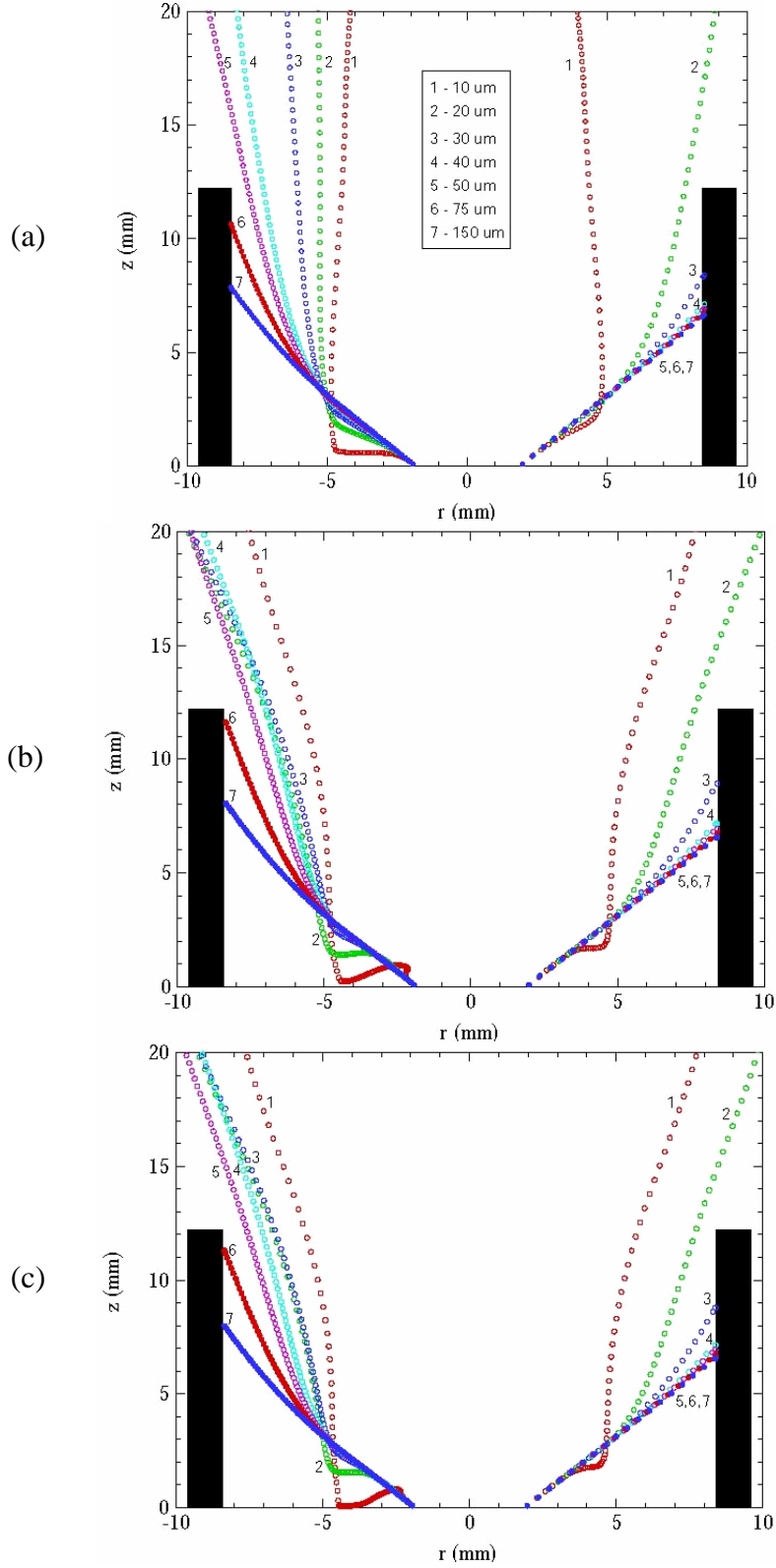


Fig. 6 Trajectories of non-evaporating droplets injected at $r_{inj} = 2$ mm for a cold turbulent flow with three different swirl modes: (a) no-swirl, (b) co-swirl, and (c) counter-swirl. In each figure, trajectories are shown for injection velocities of 5 and 20 m/s on the left and right side of the central line, respectively.

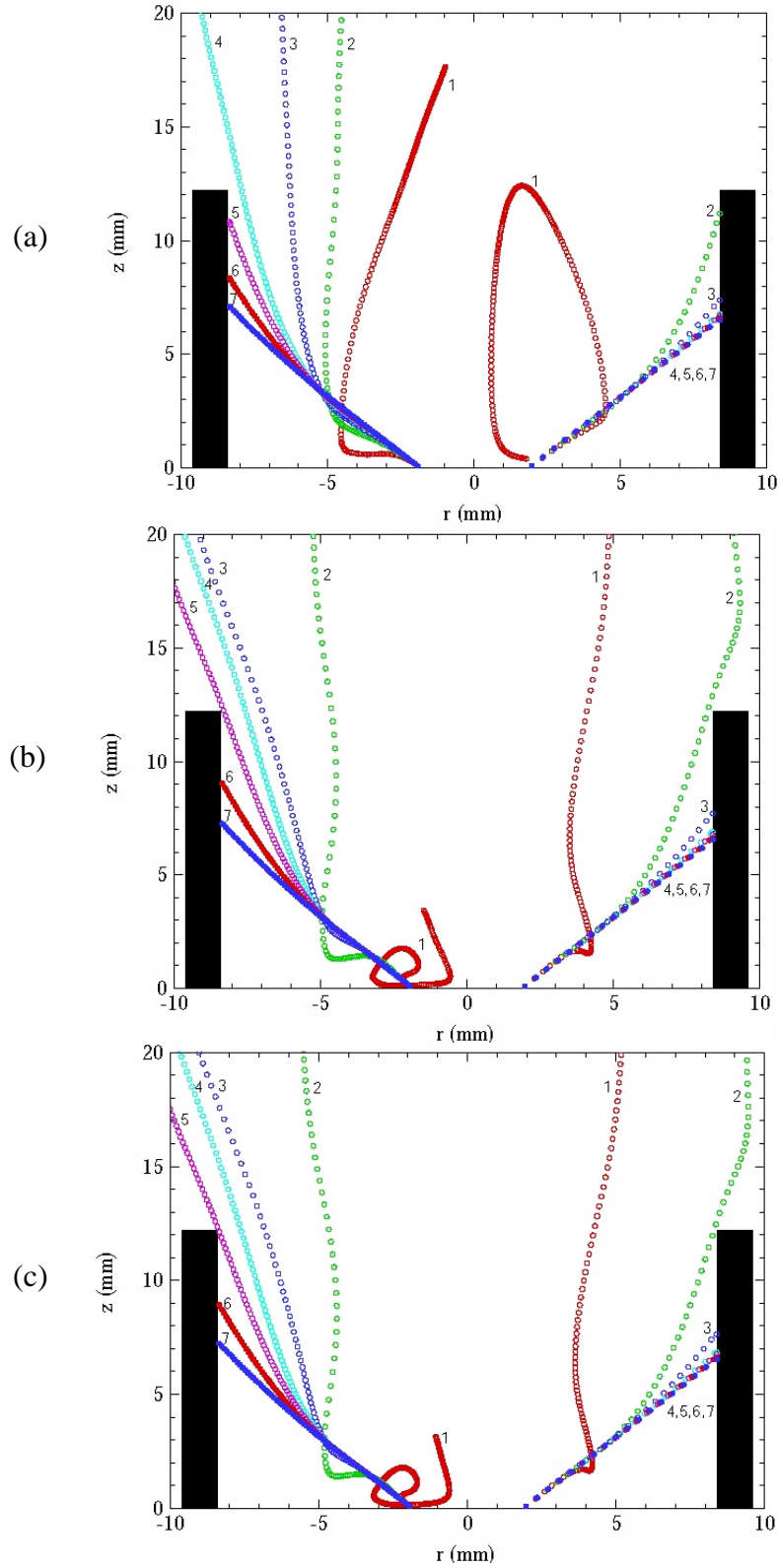


Fig. 7 Trajectories of evaporating droplets injected at $r_{inj} = 2$ mm for a hot turbulent flow with three different swirl modes: (a) no-swirl, (b) co-swirl, and (c) counter-swirl. In each figure, trajectories are shown for injection velocities of 5 and 20 m/s on the left and right side of the central line, respectively.

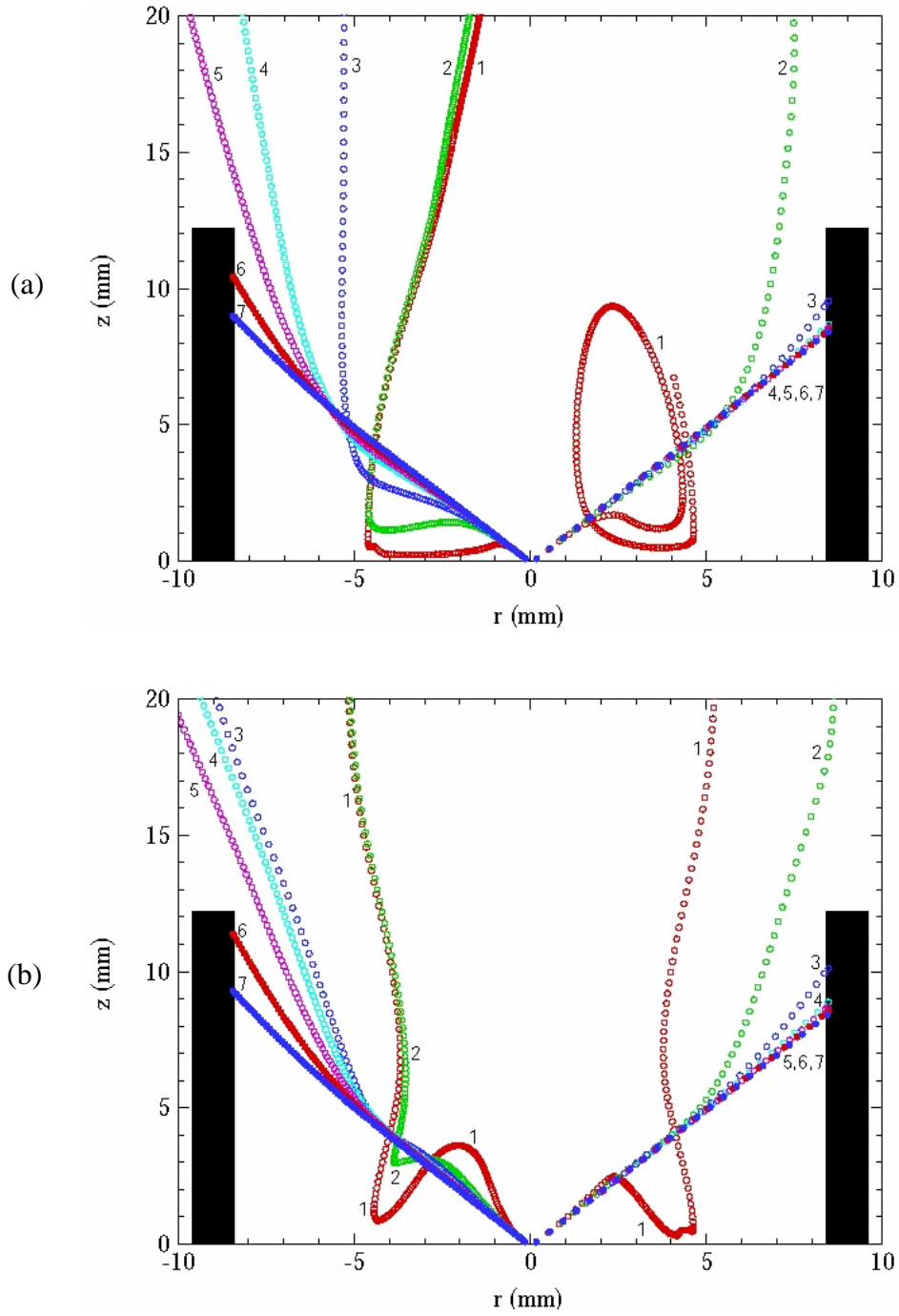


Fig. 8 Trajectories of evaporating droplets injected at $r_{inj} = 0.2$ mm for a hot turbulent flow with two different swirl modes: (a) no-swirl, (b) counter-swirl. In each figure, trajectories are shown for injection velocities of 5 and 20 m/s on the left and right side of the central line, respectively.